DAMAGE SENSING ENHANCEMENT IN POLYMER-REGOLITH-CNT COMPOSITES VIA EXPOSURE TO UV RADIATION–FOUNDATIONAL WORK

Joseph Cunningham
Advisor: Dr. Gary D. Seidel
Virginia Polytechnic Institute and State University, Blacksburg, VA 24060

Abstract

The Artemis missions have increased the urgency with which new materials and technologies relevant to Lunar exploration must be developed. This research addresses the need for construction materials which allow for stability, damage sensing, and inclusion of native filler materials. Damage-sensing is enabled by incorporation of carbon nanotubes (CNTs) into a polymer matrix, and this paper details initial steps in determining if this potential persists when Lunar regolith simulant is used as filler. Preliminary damage sensing results from ASTM D695 samples of regolith simulant mixed with 1% CNT by weight PDMS matrix in an 88/12 ratio is discussed. Sample compression occurred at 1.3 mm/min while an LCR meter passed 10kHz, 2V AC through attached electrodes. Resistance and reactance changes were measured and correlated with strain and damage identified by stress-strain relationships. Strain sensing capability similar to other CNT material systems was discovered, though material tailoring will need to be carried out to allow for viable damage sensing. The development of the custom UV exposure chamber necessary to test UV enhancement of damage sensing capabilities is discussed. Finally, a computational model based on Eshelby's equivalent inclusion approach is detailed and applied to data from previous studies to confirm viability.

Introduction

The Artemis program and upcoming crewed landings at the Lunar South Pole have provided increased impetus for research and development of materials and structures focused on enhancing safety and decreasing cost of long-term missions to the Moon[1]. A primary method of increasing structural safety and maintainability is through incorporation of self-sensing properties into materials applied to Lunar construction projects[2]. Use of in situ resources (ie. Lunar regolith) as a major component in such structures serves to decrease the mass, and thus the cost, of material transportation to the Moon from Earth[3].

Incorporating low mass fractions (1-2%) of carbon nanotubes (CNTs) into polymer matrices has been shown to enable strain- and damage-sensing via monitoring of changes in resistance and reactance[4–7]. This method has been proven in polymer-bonded composites (PBCs) including those with high mass fractions of mock-energetic[6,7] and silicate[8] fillers. The creation of self-sensing potential in high-silicate composites is especially relevant to this research, as silica composition of Lunar highlands regolith sits near 45%[9].

Contemporary research into Polymer-bonded Regolith Composites (PBRCs) emphasizes gross mechanical properties (flexural strength, modulus, impact resistance) relative to regolith weight percentage (typically JSC-1 simulant). Flexural strengths of PBRCs tend to increase with binder content but vary from 5 to 35 MPa depending on binder type, percentage, and processing[10],and composites of epoxy resin and inorganic fillers (of which Lunar regolith is a subcategory) have been found to have compressive strengths of between 17-60 MPa with varying binder contents[11], putting both metrics on par with common terrestrial building materials[10,11]. While inclusion of CNTs has been touched upon or recommended[12], no such PBRCs have been created, tested, or analyzed for damage sensing capabilities. This paper will demonstrate a proof-of-concept run in fabrication and testing for self-sensing of a PBRC including CNTs.

The Eshelby Equivalent Inclusion Method is used to estimate the effect on material properties of differing shapes and concentrations of ellipsoidal inclusions embedded in a homogeneous matrix (or effective matrix). As such, it can estimate the change in elastic modulus experienced as a material is damaged, where this damage is modeled as an increasing percentage of ellipsoidal voids in the material[13]. Through application of an inverse problem approach[14], this method can be used to estimate the amount of damage within a sample from the change in modulus experienced during testing. In turn, this can be correlated with the electrical readings to refine understanding of precision of self-sensing capabilities of the composites in question.

Inclusion of small amounts of CNTs in polymer matrices has also been shown to mitigate matrix degradation under exposure to ultra-violet (UV) light (a major environmental concern on the Lunar surface due to lack of an insulating atmosphere[15]) through formation of stable, entangled surface networks of nanotubes[16]. Such networks are also responsible for the previously mentioned self-sensing capabilities[4]. Due to the similarity in conductive potential of these networks, the main goal of this research is to determine if UV-instigated CNT networks may enhance the damage-sensing capability of polymer composites generally, and polymer-bonded regolith composites (PBRCs) in particular.

Methodology

Three main research foci have been pursued relative to planned research goals. Preliminary samples were created to validate the ability of available facilities and apparatus to fabricate viable test blanks. A UV exposure chamber was designed and constructed to allow for irradiation of composite specimens in near-Lunar spectral conditions. Finally, a computational model was created using the Eshelby Equivalent Inclusion method[17] to allow for correlation of results and comparison to observations. The following section details the methodology used in pursuit of each of these research sub-goals.

PBRC Fabrication and Testing

Proof of concept testing and fabrication of PBRCs utilized Sylgard 184 two-part elastomer, a version of polydimethylsiloxane (PDMS)[18]. For samples not including CNTs, Part A and Part B were mechanically mixed in manufacturer recommended ratios (Part A/Part B, 10:1) before LHS-1 Lunar Highlands Simulant[19] was mechanically mixed with the PDMS binder in a ratio of 88/12 LHS-1/PDMS by weight. This mixture was then degassed for 15 minutes 90 kPa, after which it was packed into ASTM D695 compression molds before being degassed again, then cured on a hotplate for 60 minutes at 135 °C.

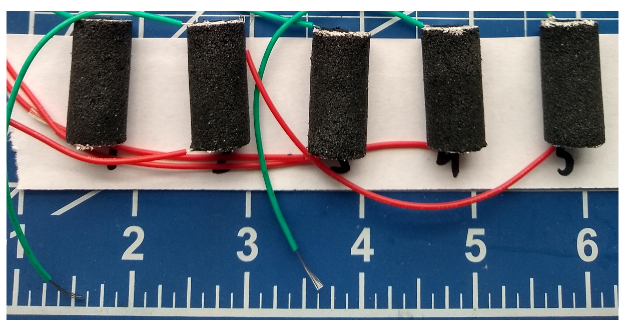

Figure 1: PDMS/LHS-1/CNT samples with attached electrodes.

Additional steps were necessary for fabrication of 1% CNT matrix (by weight) samples.The appropriate weight of PDMS part A was thinned with chloroform to allow for more even dispersion of CNTs, which were added to the mixture and mechanically stirred beneath a fume hood before being transferred to a high-shear mixer and mixed at 2000 RPM for 10 minutes. The beaker was then moved to a probe sonicator, where it was run through a 45 minute cycle with a 20 minute pulse at 75% amplitude. Once removed from the sonicator, the mixture was transferred to an evaporator, where the chloroform was removed. After this process was completed, PDMS Part B was added and the fabrication followed the same format as previously noted. Fully prepared samples, including attached electrodes, can be seen in Fig. 1.

Electrodes were attached to the top and bottom of each cylindrical compression sample using silver conductive epoxy and conductive paint to facilitate electrical measurements. Mechanical testing was performed on an Instron uniaxial testing rig with a crosshead displacement rate of 1.3 mm/min (see Fig. 2). The steel grips were insulated with electrical tape and samples were connected to an LCR meter where a 10 kHz frequency at 2 V AC was applied. Baseline resistance and reactance for preloaded samples were noted, and compression tests were carried out concurrent with electrical data recording through failure of the samples. Results were analyzed in MatLab.

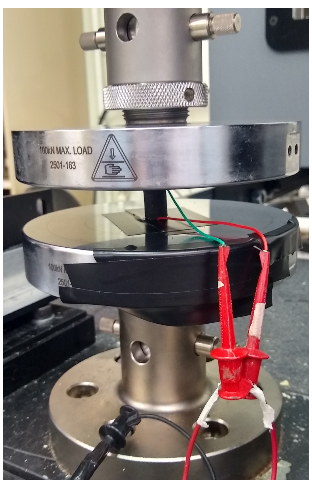

Figure 2: PBRC sample in Instron uniaxial testing rig. Note electrodes attached to sample top and bottom.

UV Chamber Development

UV exposure at 1 AU (100-400 nm wavelength range)[20] is estimated at 107 (W/m^2)[21]. Safety, financial, and technical constraints limit the experimental UV exposure range to above 290 nm with UV emissions from 290-400 nm, which are comparable to spectra used to generate entangled surface CNT networks[16]. These wavelengths have photon energies from $4.97 * 10^{-19}$ to $6.85 * 10^{-19}$ J[22], which may break covalent bonds with energies of 299-413 kJ/mol. The selected polymers have bond energies in this range (318-602 kJ/mol)[23–25], making degradation and surface network growth likely. Effects in epoxy will likely be greater than in PDMS, as epoxy C-C and C-O backbone bonds fall within the photon energy range of the exposure spectrum. Si-O bonds in the PDMS backbone are unlikely to be affected, though sidechains (Si-C) may be broken[23,26].

The custom UV exposure chamber (Fig. 3) was designed to allow specimen irradiation at the aforementioned wavelengths. Compact fluorescent bulbs in parabolic reflectors illuminate a center shelf where samples experience bi-directional exposure.

Bulbs were selected based on both intensity and spectral similarity to space UV in the 290-400 nm range[21,27]. Estimated irradiance at the shelf center is over 244 W/m2 in this UV band, and at this intensity the 200 MJ/m2 dosage required for CNT surface network formation[16] should be achievable in less than 10 days.

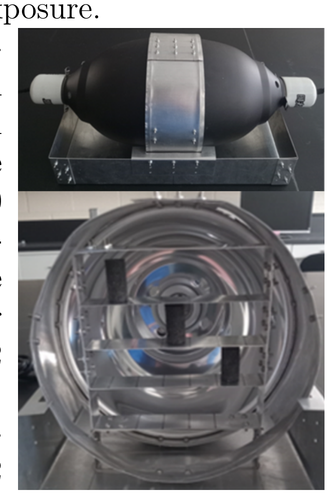

Figure 3: Custom UV exposure chamber exterior (top) and interior with shelf (bottom) and ASTM D695 compression samples.

Eshelby Equivalent Inclusion Model

The Eshelby equivalent inclusion method is used to simulate composites consisting of multiple phases which may include voids, including those representing sustained damage[17]. Voids decrease sample stiffness, which can be used to estimate initial void percentage or damage propagation during sample testing. The model developed assumes three solid, isotropic filler types, included in roughly the proportions found in LHS-1: silica (SiO_2), alumina (Al_2O_3) and calcium oxide (CaO)[19]. These inclusions are assumed to be ellipsoidal, with principal half-axis lengths between 5-100 um (per LHS-1 particle diameter distributions[19]). These solid particles are embedded in the matrix (binder) phase, either PDMS or epoxy. Initial voids are modeled using disk-shaped inclusions ($thickness/radius = 1/10$), as these likely form during sample creation, and damage-induced voids are simulated with similar geometry ($thickness/radius = 1/100$). Finally, all inclusions, solid and void, have principal axes oriented to the primary axes of the test specimen (i.e., compressive axis of specimen oriented with thickness of voids and one principal axis of ellipsoids) for ease of simulation construction and computational efficiency, though a more comprehensive model may be developed to allow for variation of orientation (Fig. 4).

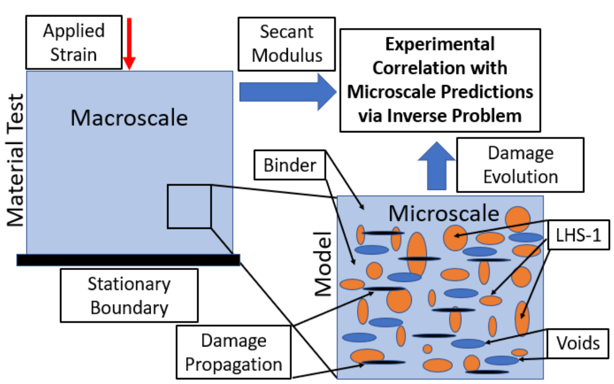

Figure 4: Graphical explanation of damage correlation computational model.

The current model can be tailored in several ways. Any number of randomly selected ellipsoidal half-axes within range can be selected, tailoring repeatability and simulation runtime. The model estimates the initial percentage of voids based on a comparison of experimentally measured modulus with that expected from a solid sample with void inclusions, from which an initial proportion of nascent voids is determined. This will allow model verification through measurement of voids noted in electron micrographs. Initial voids can be specified as either spherical or disk-shaped, with disk-shaped voids giving an initial estimate closer to expected behavior in compression samples. This estimate is applied to the simulated sample as an empty inclusion, and in addition to the solid inclusions, is used to correlate the change of modulus with damage. Secant moduli are measured from the experimental data, and these are matched with corresponding expected damage from the computational model, yielding an estimate of damage propagation over the testing regime. It is anticipated that matrix properties can be modified to account for inclusion of CNTs, as they will be added in an unoriented form, leading to a roughly homogeneous mixture affecting bulk matrix properties.

Results

Preliminary results for the above-mentioned sub-categories have been obtained. Sample sets of PDMS-LHS1-CNT compression blanks were tested to failure while electrical data was gathered, and this information was analyzed in MatLab. The UV chamber was calibrated based on sensor voltages and measured temperatures, yielding a mapping of relative irradiation intensities at the sample shelf. Finally, the Eshelby inclusion model was tailored to expected sample composition and results correlated with those from previously published papers.

PDMS-LHS1-CNT Proof of Concept

Sample fabrication and mechanical and electrical testing were executed for multiple sets of 5 samples for both PDMS and epoxy PBRCs without UV exposure (testing setup shown in Fig. 2). Collection of electrical data from epoxy PBRC samples proved difficult due to composite strength and stiffness leading to breaching of the insulation covering the testing rig sample platforms, grounding the electrodes and invalidating electrical readings.

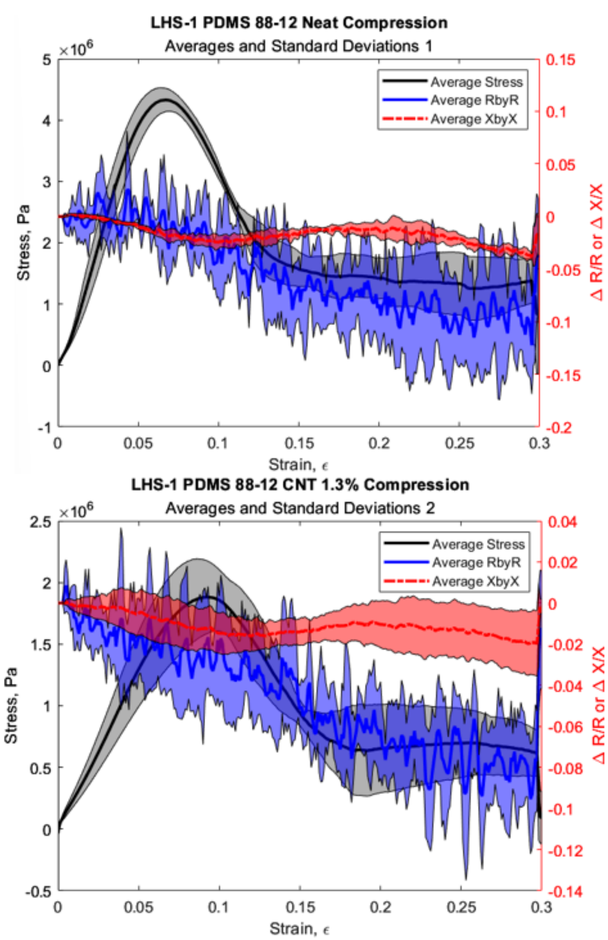

Figure 5: Mechanical and electrical test results for PBRC w/o CNTs (top, NEAT) and CNT-PBRC (bottom).

LHS-1/PDMS/CNT PBRC compression set results are shown in Fig. 5. Shaded regions show single standard deviations from the mean (solid lines) values for stress, normalized resistance change ($\Delta R/R$) and normalized reactance change ($\Delta X/X$). The NEAT set (top) contains no CNTs, while the CNT set (bottom) contains 1.3% CNTs relative to binder weight. Samples were tested at 12% binder weight to determine if this composition showed reasonable material properties and adequate potential for self-sensing capabilities. Electrical data suggests strain sensing via resistance (consistent decrease), though damage sensing is inconclusive. Readings do not change significantly with added CNTs, suggesting insufficient CNT content in the applicable composite. The stress plateau between strain values of 0.15 and 0.3 in both sets is evidence of crumbling due to significant presence of voids, a fact confirmed by SEM imaging (Fig. 6). This void concentration likely contributes to depressed mechanical properties as both modulus (81 MPa for NEAT and 26 MPA for CNT) and max stress (4.1 MPa for NEAT and 1.9 MPA for CNT) are lower than expected. The lower values for CNT specimens are likely due to differences in fabrication method between specimen types.

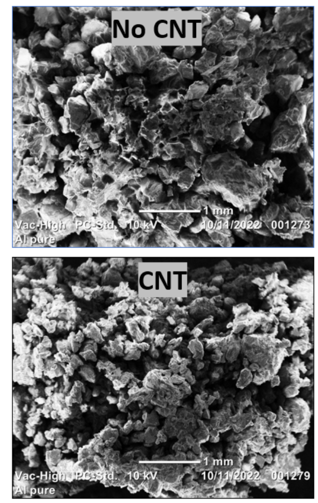

Figure 6: Electron micrographs of no CNT (top) and CNT (bottom) PBRCs showing void presence.

UV Chamber Performance

Due to difficulties with absolute calibration imposed by lack of funding and apparatus, actual irradiance values were not obtained. However, relative irradiance at various positions was gathered via use of UV sensors, while temperature data at these positions was obtained through use of thermocouples attached to each sensor mount. Irradiance distribution was assumed symmetric about the vertical plane of the sample exposure shelf. A temperature-correlated baseline irradiance distribution (reference temperature 50 °C) was found for the interior of the chamber at the estimated exposure distance of samples (Fig. 7) in terms of the voltage output of each sensor (minus applicable dark current at that sensor position).

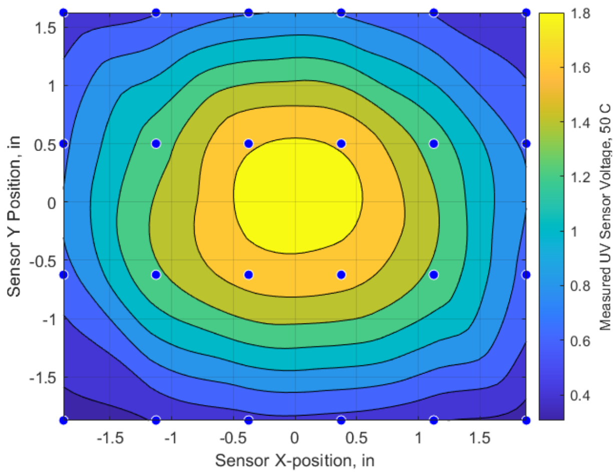

Figure 7: Irradiance distribution within UV exposure chamber, in terms of sensor voltage. Blue dots represent the estimated centers of exposed samples.

A sample location rotation was generated to allow for +/- 5% variation in irradiance during the overall exposure cycle. Initial exposures of 288 hrs have been carried out, with 1/4 rotation after 72 hrs, sample positions changed after 144 hours, another 1/4 rotation after 216 hours, and completion of the exposure at 288 hours. UV sensors are used throughout exposures to monitor chamber performance and detect major drops in voltage which could signal bulb burnout or malfunction, allowing for corrective action to achieve the desired dosage. The irradiance of applied bulbs was also found to decrease by 4-14% after a full exposure cycle of 288 hours.

Eshelby Model Preliminary Validation

Figure 8 shows a comparison of results from an example using experimental data from a previously tested PDMS-LHS-1 specimen (bottom) with electrical data from previous tests of 80% filler specimens (top)[6]. The lower image is shown to allow comparison between the estimated damage of the computational model and expected electrical readings (in the form or $\Delta R/R$ and $\Delta X/X$)typical of damage sensing present in the top image. The example model simulated fifteen sizes of ellipsoidal inclusions embedded in a PDMS matrix. Estimated initial void content in the specimen ranged from 18-24%.

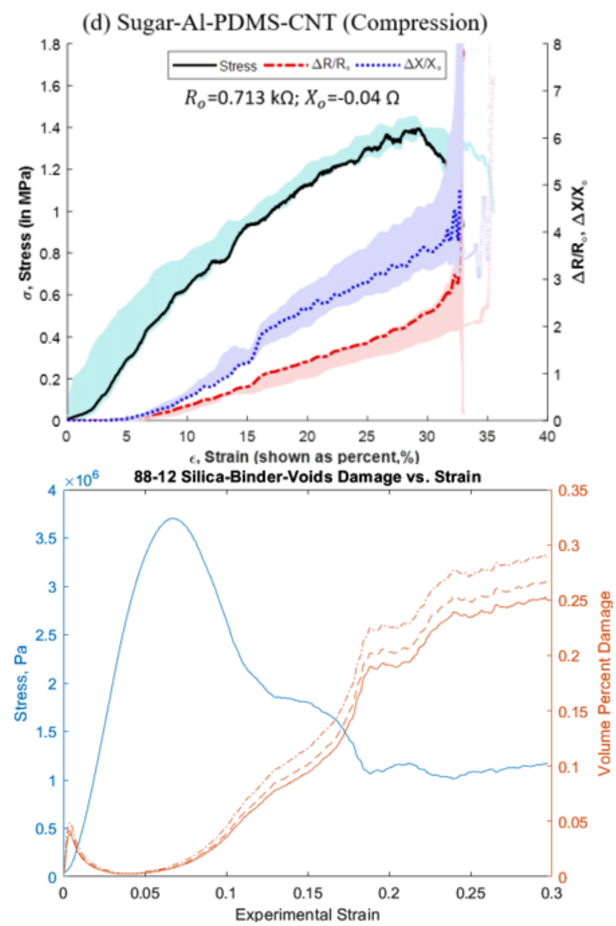

Figure 8: Preliminary validation and analysis of Eshelby damage model.

Three separate simulation runs are represented by the various percent damage lines (Fig. 8, bottom, red), which show variation due to the randomization of ellipsoidal inclusion dimensions. Both the estimated damage from the bottom chart and the normalized electrical data from the top chart show a series of bumps which may correlate to periods of rapid damage propagation, as well as a significant upsweep in these measurements (noted 17% strain in the damage estimate and 32% in the illustrated electrical data). While these two data sets cannot be directly compared due to differences in composition, it is hoped that a close correlation will be identified between the modeled damage estimate as the model matures and electrical data is collected from samples with correlated compositions.

Conclusions and Future Work

From the aforementioned results, it was concluded that strain and damage sensing in PBRCs including CNTs is feasible, given several modifications. While strain sensing is apparent even at the very high mass loadings of regolith tested, it will be necessary to increase both the overall binder and CNT content to allow for adequate conductivity for reliable damage sensing. Porosity estimates have been revised to 30% by volume (up from 23%) for loose LHS-1, increasing the amount of binder necessary to fill these voids to 20% by weight. The additional adhesion supplied should remedy the crumbling noted in previous test runs and increase mechanical properties. This increased binder composition will also boost CNT content by at least 50%, allowing for decreased electrical noise and increased sensitivity in CNT samples enabling sensing of both strain and damage. The frequency of the A/C current applied will be raised from 10 kHz to 100 kHz, also decreasing noise in sample measurements. The fabrication method has been modified and tested to allow for a more reliable comparison between pure and CNT-rich samples. In addition, rigid aluminum plates layered with insulative material to separate conductive electrodes from metal testing rig grips have been verified to provide adequate insulation and strength for testing of both epoxy and PDMS samples. These methods are increasing the comparability of both Epoxy and PDMS sample sets.

While the viability of the custom UV chamber for execution of long exposures has been proven, work remains to be done for correlation of CNT network formation relative to exposure time. Sample labeling and placement methodologies have been refined to allow for precise tracking of individual samples relative to exposure intensities and effects, as well as minimization of damage to any created CNT networks. Due to the drop in bulb irradiance over the course of a single cycle, new bulbs will be used for each exposure to allow for the greatest irradiance possible.

The Eshelby computational model requires refinement and direct application to PBRC testing data to be fully validated for this research. While initial results are promising, geometry, rotations, and volume percentages of both void and material inclusions must be revisited and revised to allow for closer prediction of experimental results. In addition, more accurate material properties for LHS-1 components must be obtained, and methods of dealing with non-isotropic crystalline materials may be considered to increase accuracy.

Acknowledgements

This research was made possible by the assistance and support of many experts. The author would like to thank Dr. Gary D. Seidel for training in the Eshelby method and use of various lab techniques and equipment, access to and use of the Aerospace Structures and Materials Laboratory and included materials, and general research support and evaluation. Viswajit Talluru and Nishant Shirodkar were of great assistance in application of best practice lab and instrumentation methodologies, as well as in supervision of and training with these techniques. Zoe Landsman and Jared Long-Fox from Exolith Labs provided detailed information on the composition of the LHS-1 regolith simulant used in this study. Finally, the author would like to acknowledge the help of Dr. Elena Lind as well as Bill, Carter, and Mike from Adafruit Support and users Dastels and poven on the Adafruit discussion boards who greatly assisted with the setup and characterization of the UV chamber sensor suite.

The author would also like to acknowledge the financial support for this research obtained from the Virginia Space Grant Consortium Graduate STEM Research Fellowship and the Joseph Frank Hunkler Memorial Scholarship.

Works Cited

[1] C. W. Warner. Lunar Living: NASAs Artemis Base Camp Concept. URL: blogs.nasa.gov/artemis/2020/10/28/lunar-living-nasas-artemis-base-camp-concept/. (published: 10.28.2020).

[2] National Aeronautics and Space Administration. NASA Technology Roadmaps TA 10: Nanotechnology. URL: nspires . nasaprs . com / external / viewrepositorydocument / cmdocumentid=896240/solicitationId=%5C % 7B4C4796B7 - 1D86 - C986 - 49E5 - A76ABB0A9EAE % 5C % 7D / viewSolicitationDocument = 1 / 2015 _ NASA _ Technology _ Roadmaps _ TA10 _ Nanotechnology . pdf. (published: 07/2015).

[3] National Aeronautics and Space Administration. In-Situ Materials Challenge. URL: nasa . gov / feature / in - situ - regolith - modular - structural - element - system - challenge. (published: 10/2015).

[4] N. Shirodkar and G. D. Seidel. "Strain and damage sensing of polymer bonded mock energetics via piezoresistivity from carbon nanotube networks". In: AIAA SciTech Forum. Orlando, FL. 2020.

[5] S. Shirodkar N.and Rocker and G. D. Seidel. "Strain and damage sensing of polymer bonded mock energetics via piezoresistivity from carbon nanotube networks". In: Smart Materials and Structures 28 (Sept. 2014).

[6] N. P. Shirodkar. "Leveraging Carbon based nanoparticle dispersions for fracture toughness enhancement and electro-mechanical sensing in multifunctional composites". PhD thesis. Virginia Polytechnic Institute and State University, 2022.

[7] J. J. Ku-Herrera, F. Aviles, and G. D. Seidel. "Self-sensing of elastic strain, matrix yielding and plasticity in multiwall carbon nanotube/vinyl ester composites". In: Smart Materials and Structures 22 (2013).

[8] A. Garner et al. "Monitoring Fatigue Damage in PC using Carbon Nanotubes". In: Advanced Materials Research 1129 (2015), pp. 94–101.

[9] S. R. Taylor. Lunar science: A post-Apollo view. Pergamon Press, Inc, 1975.

[10] B. J. Chen T.and Chow et al. "Inorganic-organic hybrid of lunar soil simulant and polyethylene". In: Journal of Materials in Civil Engineering 28 (4 2016).

[11] M.Z. Naser. "Space-native construction materials for earth-independent and sustainable infrastructure". In: Acta Astronautica 155 (2019), pp. 264–273.

[12] M. Isachenkov et al. "Regolith-based additive manufacturing for sustainable development of lunar infrastructure An overview". In: Acta Astronautica 180 (2021), pp. 650–658.

[13] G. D. Seidel. Eshelby Inclusion Problem, Eshelby Equivalent Concentration Tensors, and Micromechanics Effective Lamina Properties. 2022.

[14] A. Tarantola. Inverse Problem. (cited: 10/2022). URL: mathworld.wolfram.com/InverseProblem.html.

[15] J. B. Awaja F.and Moon et al. "Surface molecular degradation of 3D glass polymer composite under low earth orbit simulated space environment". In: Polymer Degradation and Stability 95 (6 2010), pp. 987–996.

[16] T. Nguyen et al. "Impact of UV irradiation on multiwall carbon nanotubes in nanocomposites: Formation of entangled surface layer and mechanisms of release resistance". In: Carbon 116 (2017), pp. 191–200.

[17] T. Mura. "Isotropic Inclusions". In: Micromechanics of Defects in Solids. Boston: Martinis Nijhoff Publishers, 1987.

[18] Dow. SYLGARD 184 Silicone Elastomer Kit. (cited: 02/2023). URL: dow.com/en-us/pdp.sylgard-184-silicone-elastomer-kit.01064291z.html#overview.

[19] Exolith Labs. LHS-1 Lunar Highlands Simulant: Fact Sheet. URL: cdn.shopify.com/s/files/1/0398/9268/0862/files/lhs-1-spec-sheet-Dec2022.pdf?v=1670609567.

[20] World Health Organization. Radiation: Ultraviolet (UV) radiation. Mar. 2016. URL: http://who.int/news-room/questions-and-answers/item/radiation-ultraviolet-(uv) (visited on 10/22/2022).

[21] Solar Constant and Zero Air Mass Solar Spectral Irradiance Tables. Standard. American Society for Testing and Materials, 2019.

[22] PVEducation. Energy of Photon. URL: http://pveducation.org/pvcdrom/properties-of-sunlight/energy-of-photon (visited on 10/26/2022).

[23] C. Yoder. Common Bond Energies (D) and Bond Lengths (r). 2022. URL: http://wiredchemist.com/chemistry/data/bond_energies_lengths.html (visited on 10/22/2022).

[24] University of Michigan. PDMS. Apr. 2020. URL: http://lnf-wiki.eecs.umich.edu/wiki/PDMS (visited on 10/22/2022).

[25] ChemicalBook. Bisphenol F Diglycidyl Ether. 2022. URL: http://chemicalbook.com/ChemicalProductProperty_EN_CB7672361.htm (visited on 10/22/2022).

[26] D. De Rooij. Energy of a Photon. URL: http://sinovoltaics.com/learning-center/basics/energy-of-photon/ (visited on 10/22/2022).

[27] ExoTerra. Sales Sheet Reptile UVB NA-EU. 2013. URL: http://exo-terra.com/en/products/reptile_uvb200.php (visited on 03/23/2022).